13th ewtec 2019 Proceedings of the 13th European Wave and Tidal Energy Conference 1-6 Sept 2019, Naples, Italy

Design and optimization of hydrofoils tailored for marine current turbines

Francisco Espenica, Ricardo B. Santos Pereira, Gael L. Oliveira Andrade, João Baltazar and José A.C. Falcão de Campos

Abstract— **The present study describes a novel design strategy of hydrofoils tailored for marine current turbines. The designation of the newly proposed foil sections is IST-MT1-XX. The hydrofoils are designed with an existing optimization framework, which uses CST for the foil geometry parametrization and a viscous-inviscid panel code to estimate foil hydrodynamic performance. The optimization challenge is formulated as a multi-objective problem and is solved with the NSGA-II genetic algorithm. Two specific hydrofoil performance cost functions (CF) are defined as design goals: CF1 relates to hydrodynamic performance; CF2 refers to cavitation performance. Both CF1 and CF2 simulate the conditions experienced at different horizontal axis turbine blade sections during operation. The performance of each candidate hydrofoil incorporates both natural and forced transition flow regimes, for Reynolds numbers set to match those of a reference marine current turbine. CF1 simultaneously maximizes the optimal lift coefficient and lift to drag ratio at the optimal angle of attack, considering both flow regimes. The performance of each candidate hydrofoil is compared with the performance of reference hydrofoils of series NACA 63-8XX and 66-8XX. Results of the hydrofoil optimization display similar trends for all blade spanwise sections and correspondent relative thicknesses evaluated. Specifically, results show that hydrofoils with higher cavitation margin have a smaller camber and maximum thickness chordwise location farther from the leading edge. The novel sections outperform the reference hydrofoils, as increases in maximum lift to drag ratio and optimum lift coefficient for both natural and forced transition regimes are achieved, as well as cavitation margins of up to 3 relative to the local cavitation number.**

Keywords – **tidal energy, marine current, hydrofoil, design, optimization**

I. Introduction

WORLDWIDE energy consumption has been continuously growing due to increasing global population and technological development. Large progress has been made in the fields of solar and wind energy production, making these the most developed renewable energy production sources available and viable today [1]. However, these sources are subject to monthly and daily variations due to the weather, making their availability hard to predict. This unpredictability and relative randomness make this type of energy production unsuitable for sustaining the continuous base load energy demand currently provided by traditional fuel, carbon-based sources. Due to these limitations and with environmental and sustainability concerns in mind, research has been conducted in recent years in the area of ocean energy [2].

Tides are influenced by the gravitational interaction of the Earth-Moon-Sun system and are mostly independent of weather conditions, making it possible to predict resource availability with decades' notice and very high accuracy [3]. This characteristic is unrivalled by any other renewable energy source. The horizontal-axis current turbine (HACT) appears to be the most technologically and economically viable tidal energy harnessing technology currently available [4],[5], generating power from currents created through tidal movement.

One of the most important components that constitute a turbine are the rotor blades. These components generate lift and are responsible for the exchange of momentum between fluid and rotor. Each blade section has a geometry which corresponds to a hydrofoil. The use of different hydrofoils can make the extracted power of a HACT vary significantly, even under the same operating conditions [4]. Important hydrodynamic characteristics of hydrofoils include the pressure distribution over the hydrofoil surface and integrated quantities lift coefficient C_L and drag coefficient C_D. Perhaps the most important requirement for an HACT is the avoidance of cavitation, which must be tackled directly in the design stage of both hydrofoil and blades and has to be achieved while maintaining high L/D ratio, delaying separation and stall, over a wide range of angles of attack and flow conditions.

With these considerations in mind, the present study aims to develop a hydrofoil design procedure employing an already existing foil optimization framework [6]. Cost functions are developed towards the goal of improving the hydrodynamic performance of the hydrofoils while also decreasing the risk of cavitation. The present article concerning hydrofoil design was developed in close connection with a marine turbine blade planform design [7].

Section II offers a brief description of the optimization environment. Section III elaborates on the optimization

ID: 1638, track: THM
This work was supported by FCT/MCTES (PIDDAC) through project UID/EEA/50009/2019
F. Espenica was with Instituto Superior Técnico (IST) as MSc researcher, Av. Rovisco Pais, 1, 1049-001, Lisboa (email: francisco.espenica@tecnico.ulisboa.pt)
R.B. Santos Pereira is an assistant professor at IST, Av. Rovisco Pais, 1, 1049-001, Lisboa, and TUDelft, Mekelweg 5, 2628 CD Delft, Netherlands (email: ricardosantospereira@tecnico.ulisboa.pt)
G. L. Oliveira Andrade is a PhD researcher at TUDelft, Mekelweg 5, 2628 CD Delft, Netherlands (email: gaeldeoliveira@gmail.com)
J. Baltazar is a researcher at IST, Av. Rovisco Pais, 1, 1049-001, Lisboa (email: joao.baltazar@ist.utl.pt
J. A. C. Falcão de Campos is associate professor at IST, Av. Rovisco Pais, 1, 1049-001, Lisboa (email: falcao.campos@tecnico.ulisboa.pt)

setup and the definition of the specific hydrofoil performance cost functions. Section IV shows the optimization results, and section V presents hydrofoils IST-MT1-XX, selected from the optimization results. Finally, section VI states the main conclusions.

II. Optimization environment

In this section the design and optimization procedure as well as the simulation specifications are briefly described.

A. Optimization tool – Optiflow

The procedure used for this study was originally conceived as a new airfoil design strategy, relying on the mathematical description of the foil shape with *CST* parametrization [8] and the NSGA-II multi-objective optimization algorithm to render optimal compromises between design goals. This optimization tool is here adapted to the design and optimization of hydrofoils, having been extensively used and proven effective for the design of optimized sections for wind energy applications (airfoils) [9],[10]. The following subsections offer brief descriptions of several aspects concerning the optimization tool's characteristics and inner workings. For more detailed information the reader is referred to [6], [10] and [11].

1) Optimization framework

Optiflow is an optimization framework implemented in the *MATLAB* computing environment. Its code is built around an object-oriented data structure and relies on Symbolic Computation, Spline and Global Optimization toolboxes. The code's objects are designed following a team paradigm, meaning, each object can be conceived as a worker within a team which then calls on other "workers" (objects) to execute tasks they are specialized in, namely:

- system_context - handles interaction with operating system and hardware;
- simulation_worker - executes simulations in *RFOIL* or *XFOIL* and requests shape generation;
- shape_definition - stores and uses information about the airfoil shape, using two parametrization objects (one for each side of the foil);
- global_cost_function - evaluates the complete cost function, reconditioning optimizer requests, handing simulations to the simulation worker and their results to the interpretation functions;
- gamultiobj_manager - sets up and controls execution of the optimization algorithm.

Evaluation of the cost function essentially involves evaluating the performance, or quality of the foil. This includes generating its geometry, writing a command file for *R/XFOIL*, executing the simulation, acquiring the data and interpreting the polar. The calculation of the candidate foils' polars is the most complex and time-consuming operation in the optimization process and is executed through parallel processing, having been executed on 64 virtual cores simultaneously [6] on previous studies. This framework allows for several "experiments" on the same airfoil within the same optimization loop, *i.e.* evaluate foil performance for natural and forced transition. Although it is not considered in the present study, it is also possible to consider flow control actuation on the (air)foils within the current optimization framework.

2) Geometry parametrization

The Class Shape Transform *CST* parametrization method was developed at Boeing and is presented in detail in reference [8]. The airfoil (or hydrofoil) shape is represented as the product of two functions, a class $C_{(x)}$ and a shape $S_{(x)}$ function, summed with a trailing edge thickness function $z_{(x)}$:

$$t = S_{(x)}C_{(x)} + z_{(x)} \tag{1}$$

Each side (upper-lower) of the airfoil is represented separately, as an analytical function of the relative thickness versus position, tailored with parameters that define the shape. The class function provides the base airfoil shape, and the shape function is used to perturb the class function, thereby specifing the geometry. The additional trailing edge thickness function allows for thick trailing edges to be represented accurately. The class function is a simple analytical function providing the essential features of an airfoil shape, and is defined as:

$$C_{(x)} = (1-x)\sqrt{x} \tag{2}$$

In the *CST* method as presented in [8], the shape function is a Bezier curve, meaning, a weighted sum of Bernstein polynomials; these polynomials are the basis functions used to generate the shape function $S_{(x)}$ as a linear combination with coefficients b_n:

$$S_{(x)} = \sum_{r=0}^{r=N-1} s_{(x)}^{rN}\, b_n \qquad \begin{cases} x \in [0,1] \subset \mathbb{R} \\ b_n \in \mathbb{R}^n \end{cases} \tag{3}$$

b_n is a 1-tensor holding the linear combination coefficients, and the basis functions are the complete set of Bernstein polynomials of order N and degree $N - 1$, given analytically as:

$$s_{(x)}^{rN} = \binom{N-1}{r} x^r (1-x)^{n-r} \qquad \begin{cases} r \in [0, N-1] \subset \mathbb{Z} \\ \binom{n}{r} = \dfrac{n!}{r!\,(n-r)!} \end{cases} \tag{4}$$

A Bernstein polynomial order of 8 is employed in this study, as it is sufficient to cover the airfoil design space effectively, corresponding to a set of 17 parameters describing the airfoil shape, $8_{\text{upper}} + 8_{\text{lower}} + 1_{\text{trailing edge}}$. Other geometry constraints, such as maximum and minimum camber or local thickness, are imposed based on the extreme values occurring within the set of feasible foil sections initially provided [6].

3) Hydrodynamic performance analysis tool – RFOIL

RFOIL-Suc is a fully coupled viscous-inviscid code based on *XFOIL 5*, modified [12], to account for rotational effects on blade section performance while also featuring better stall prediction. Particular effort [13] was put into

strengthening the convergence properties of *RFOIL*, used in the present formulation, resulting in greater consistency and accuracy in results when compared to *XFOIL*, even for flow without rotational effects [6]. The inviscid flow problem is solved with a potential flow model using a vortex discretization of 200 panels. The viscous problem consists in the solution of the boundary layer equations and it is coupled with the potential problem using a virtual surface transpiration approach. Despite the progress made, both *RFOIL* and *XFOIL* still suffer from limitations for the simulation of thick profiles, owing to the inherent flow-surface (small) perturbation approach used in the computation.

4) Experimental measurements and X/RFOIL calculations

In this section, some brief considerations are made regarding the numerical accuracy of the performance analysis tool *RFOIL* and why it is used instead of *XFOIL* within the optimization framework. Both tools are integrated in *Optiflow* but the performance analysis for this study (within the optimization procedure) is carried out with *RFOIL*. This comparison is made between *XFOIL 6.99* [14] and the *RFOIL* version detailed in [15], which is present within the optimization routine.

Fig. 1 and Fig. 2 show a comparison of *XFOIL*, *RFOIL* and experimental measurements of the lift and drag coefficients, C_L and C_D, respectively, versus the angle of attack AOA for foil NACA 63-815, at Re = $0.8 \cdot 10^6$. Calculations from *XFOIL* and *RFOIL* consider natural (free) transition and the N_{crit} value assumed is 4 (refer to [7] and [16]). Experimental data comes from measurements made in a cavitation tunnel by Bahaj et.al [17].

From Fig. 1 and Fig. 2 it is possible to observe that *RFOIL* results are closer to the experimental values taken for most AOAs measured and more so for high values of AOA. *RFOIL* appears to be better than *XFOIL* at predicting C_L for larger angles of attack (between 10° and 18°), as *XFOIL* largely overpredicts the experimental values.

Regarding C_D, both tools appear slightly off in their predictions, with *RFOIL* being more reliable for larger angles of attack (between 8° and 18°). This discrepancy between experimental data and *X/RFOIL* values can be partly explained by the conditions in the experimental setup, as tests did not strictly simulate two-dimensional flow [17]. Additionally, it is widely known that C_D data poses more of a challenge to obtain than C_L values, both experimental and numerically [13],[16]. Moreover, at the specific experimental *Re* and flow ambient turbulence intensity level, the transition location may be somewhat hard to predict. Nonetheless, *RFOIL* appears to outperform *XFOIL* when predicting experimental values.

Table I shows the relative difference between the maximum lift and minimum drag experimental data and values calculated by *X/RFOIL* at the same AOA. From this table we can verify the lower relative difference in the maximum C_L value prediction by *RFOIL* compared to *XFOIL*. Regarding C_D, *RFOIL* slightly overpredicts the value compared to *XFOIL*, but in Fig. 2 it is possible to observe that this tendency is inverted as predictions are made for larger AOA values (for more details regarding *X/RFOIL* the reader is referred to [6],[14] and [15]).

In light of these considerations, allied to *RFOIL*'s increased robustness when compared to *XFOIL* [6], this tool is preferred when making hydrofoil performance calculations within the optimization framework.

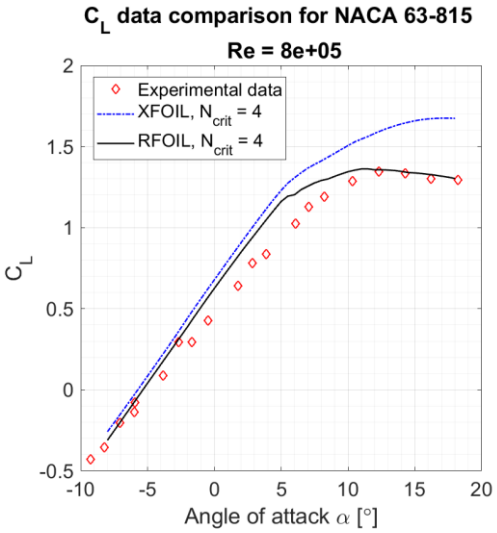

Fig. 1. Data comparison of lift coefficient C_L at Re = $0.8 \cdot 10^6$ for NACA 63-815 – experimental data from [17]

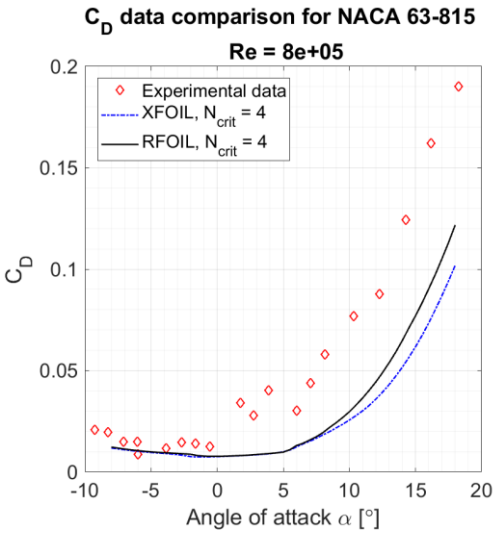

Fig. 2. Data comparison of drag coefficient C_D at Re = $0.8 \cdot 10^6$ for NACA 63-815 – experimental data from [17]

TABLE I
COMPARISON BETWEEN EXPERIMENTAL MAXIMUM C_L AND MINIMUM C_D MEASUREMENTS AND *X/RFOIL* CALCULATIONS AT THE SAME AOA

	Lift coeff. at α = 12.3° C_L [-]	Relative Difference [%]	Drag coeff. at α = - 6° C_D [-]	Relative Difference [%]
Exp. value	Max. exp. value 1.35	-	Min. exp. value 0.0088	-
XFOIL	1.59	18.4	0.0102	15.6
RFOIL	1.36	0.86	0.0105	19.2

III. OPTIMIZATION SETUP AND COST FUNCTION DEFINITION

The genetic algorithm considers 100 foil candidates per generation and each optimization run considers 50 generations. The initial "genetic" pool is composed of 40-

60 feasible (existing) foils while the remaining are randomly generated. This initial pool contains both feasible airfoils and hydrofoils, the latter having been tested and experimented as foils adequate for marine turbines in previous work, like the NACA 63-8XX [17] and S1210 [19], or marine propulsors, such as the NACA 66-8XX series [20].

Two specific hydrofoil performance cost functions, CFs, are defined as design goals. Cost function 1, CF1, relates to hydrodynamic performance, contrasting with CF2, cavitation performance. Cavitation performance is defined as the margin between cavitation number σ and the minimum pressure coefficient $C_{p_{min}}$ occurring on the hydrofoil's surface.

For each hydrofoil candidate, two lift and drag polars are calculated at a user defined Reynolds number in AOA steps of 0.5 degrees, from $-5°$ to $15°$. The first polar is obtained without prescribing the transition location (natural transition, also called free transition in this study) - this is termed the clean regime. For the second polar, transition is forced at x/c = 10% and 5% (as proposed by Timmer et.al [21]) for the lower and upper faces, respectively – referred to as rough regime. Although forcing transition is, strictly speaking, not sufficient for simulating roughness, this is the common way of simulating a soiled or rough surface on foils [21].

A unique score is attributed to each hydrofoil when considering a specific cost function. These scores are displayed in a Pareto front, which is composed by the set of design CF scores that are Pareto efficient (see Fig. 3).

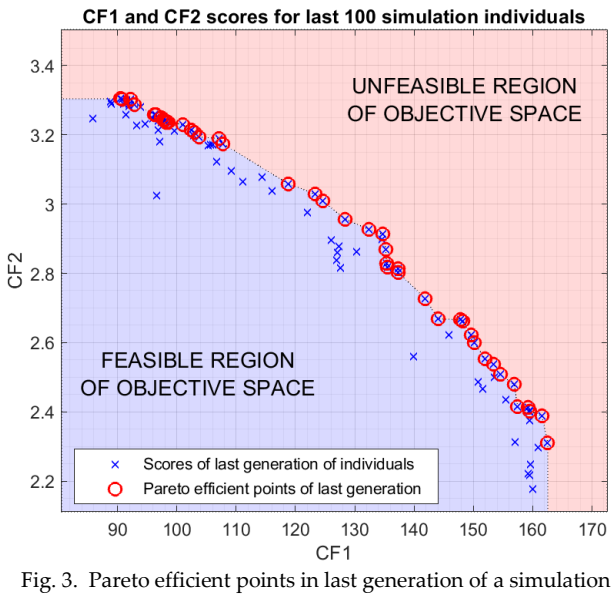

Fig. 3. Pareto efficient points in last generation of a simulation

The optimization is carried out for specific spanwise sections of a reference HACT blade and outputs hydrofoils with predefined maximum relative thickness (see refs. [7],[16] and Table II).

For the reader's better comprehension of these cost functions and corresponding results, CF2 is described first.

TABLE II
REFERENCE TURBINE DATA – RELEVANT SECTIONS FOR HYDROFOIL OPTIMIZATION – SOURCE [7],[16]

Span r/R [%]	Chord c/R [%]	Thickness t/c [%]	Reynolds Re [-]	Variation in AOA $\Delta\alpha$ [°]
20	15.0	24	$3.9{\cdot}10^6$	1.2
30	14.4	21	$4.5{\cdot}10^6$	1.3
45	11.1	18	$5.3{\cdot}10^6$	1.3
75	5.9	15	$5.5{\cdot}10^6$	1.5
100	0.7	12	$5.2{\cdot}10^6$	1.7

B. *Cavitation margin cost function – CF2*

Cost function 2, CF2, is related with the cavitation margin experienced at each blade section for each foil and is calculated as follows:

$$CF2 = \left(\sigma_{r/R}\right)_{min} - \left(-C_{p_{min}}\right)_{max} \quad (5)$$

$\left(\sigma_{r/R}\right)_{min}$ corresponds to the minimum cavitation number reached at a blade section (r/R) during its rotation, and is calculated through:

$$\sigma = \frac{p_\infty - p_v}{1/2 \cdot \rho\, V_{eff}^2} \quad (6)$$

where p_∞ corresponds to the undisturbed incoming flow pressure (static pressure), p_v and ρ are the surrounding fluid vapour pressure and density, respectively, and V_{eff} is the effective flow speed at the blade section r/R. p_∞ is calculated as:

$$p_\infty = p_{atm} + \rho g d \quad (7)$$

where p_{atm} is the atmospheric pressure; g is the acceleration of gravity and d is the depth of section r relative to the fluid's free surface - which means that calculation (6) and CF2 take the section r depth into account. For more details on these calculations, see [7],[15].

$\left(-C_{p_{min}}\right)_{max}$ corresponds to the minimum C_p value found within the range of operating angles of attack of the hydrofoil at the section, meaning:

- The AOA_{opt} is the AOA at which the foil exhibits the highest L/D value;
- C_p distribution around the foil is calculated for angles of attack ranging between $\mathrm{AOA}_{\mathrm{opt}} - \Delta\alpha/2 \rightarrow \mathrm{AOA}_{\mathrm{opt}} + \Delta\alpha/2$, being $\Delta\alpha$ the variation in angle of attack experienced at the section r/R induced by the shear of the marine current velocity profile, which affects V_{eff} and ϕ, which is the inflow angle at section r (see [7],[16]);
- The maximum value of $-C_{p_{min}}$ for this whole range, which corresponds to $\left(-C_{p_{min}}\right)_{max}$, is taken.

Through this method, a positive cavitation margin is ensured for the whole range of AOA at which a foil will operate at the given section, *i.e.* a positive cavitation margin is ensured for the totality of the blades' rotation at design conditions. If the value of CF2 is negative, cavitation will most likely occur. The C_p distribution is always calculated only for the clean regime. With forced transition, for the same AOA, the suction peak is always weaker; this happens because the turbulent boundary

layer is thicker than the laminar boundary layer, which makes the hydrofoil to be 'perceived' by the flow as having less camber, thus making the suction peak less intense.

C. *Hydrodynamic performance cost function – CF1*

The performance of each candidate hydrofoil is obtained with natural transition (no prescribed transition location) and forced transition, as previously stated. A number of versions of CF1 were tested during the optimization exercise [15], and finally it (version 5 in the figures) is calculated as follows:

$$w_1 = w_2 = 0.25 \qquad w_0 = 0.5 \tag{8}$$

$$\begin{aligned} \mathrm{AOA}_i &= \mathrm{AOA}_{opt} \\ \mathrm{AOA}_{i-j} &= \mathrm{AOA}_{opt} - \Delta\alpha/2 \\ \mathrm{AOA}_{i+j} &= \mathrm{AOA}_{opt} + \Delta\alpha/2 \end{aligned} \tag{9}$$

$$\begin{aligned} C_L^{weighted} = {} & w_1 \cdot C_L|_{\mathrm{AOA}_{i-j}} + w_o \cdot C_L|_{\mathrm{AOA}_i} \\ & + w_2 \cdot C_L|_{\mathrm{AOA}_{i+j}} \end{aligned} \tag{10}$$

$$\begin{aligned} L/D^{weighted} = {} & w_1 \cdot L/D|_{\mathrm{AOA}_{i-j}} + w_o \cdot L/D|_{\mathrm{AOA}_i} \\ & + w_2 \cdot L/D|_{\mathrm{AOA}_{i+j}} \end{aligned} \tag{11}$$

$$N = number\ of\ reference\ hydrofoils$$

$$C_L{}^{ref} = \frac{\sum_{n=1}^{N} 1.1 \cdot C_{L_n}^{weighted}}{N} \tag{12}$$

$$L/D^{ref} = \frac{\sum_{n=1}^{N} 1.1 \cdot L/D_n^{weighted}}{N} \tag{13}$$

$$C_{L_{new\ foil}}^{adim} = \left(\frac{C_{L_{new\ foil}}^{weighted} - C_L^{ref}}{C_L^{ref}} + 1 \right)^2 \tag{14}$$

$$L/D_{new\ foil}^{adim} = \left(\frac{L/D_{new\ foil}^{weighted} - L/D^{ref}}{L/D^{ref}} + 1 \right)^2 \tag{15}$$

$$\begin{aligned} CF1 = {} & 0.5 \left[C_{L_{new\ foil}}^{adim} + L/D_{new\ foil}^{adim} \right]_{free} \\ & + 0.5 \left[C_{L_{new\ foil}}^{adim} + L/D_{new\ foil}^{adim} \right]_{forced} \end{aligned} \tag{16}$$

$C_L^{weighted}$ and $L/D^{weighted}$ are values calculated (expressions (10) and (11)) by making a weighted sum of the lift coefficient C_L and L/D, respectively, over a range of angles of attack defined by (9), considering the relative weights of (8). Equations (12) and (13) calculate the mean value of $C_L^{weighted}$ and $L/D^{weighted}$ between the reference hydrofoils considered (NACA 63-8XX and 66-8XX series). Through equations (14) and (15), $C_L^{weighted}$ and $L/D^{weighted}$ of the new hydrofoil are directly compared with reference values. The "1.1" factor in equations (12)(13) and the square factor in (14)(15) direct the optimization routine to further improve the value of CF1. Finally, the value of CF1 is calculated through equation (16). This formulation intends to improve performance at both natural (free) and forced transition, *i.e.* aims to obtain hydrofoils that have a balanced performance between clean and rough regimes.

IV. HYDROFOIL OPTIMIZATION RESULTS

We start by showing the hydrofoil optimization results for relative thickness t/c_{max} of 15%, corresponding to a blade spanwise location at r/R = 0.75. Fig. 4 presents 6 subplots: on the upper left, the geometry of 15 foils selected from the Pareto front; on the bottom row, 4 plots with the L/D curve and C_L polar for natural (free) and forced transition for the 15 foils shown; on the upper right, the Pareto front with CF1 and CF2 scores for all the hydrofoils (43) resulting from the simulation (for clarity all other subplots show results for 'only' 15 foils). Red dots or lines relate to hydrofoils with higher cavitation margin, *i.e.* higher value of CF2, while blue dots or lines represent higher value of CF1. Fig. 5 displays a direct comparison with reference foils of series NACA 63-8XX and 66-8XX made by calculating the performance of the reference foils using CF1 and CF2, which means a score is attributed in the same manner for reference foils as it is for the optimized or Pareto efficient foils.

As one analyses and interprets the results, it must be stressed that choosing a hydrofoil with a larger CF1 value than another does not necessarily mean that it performs better for natural or forced transition alone. CF1 produces results in which a higher cost function value means that the overall performance, weighted between maximum

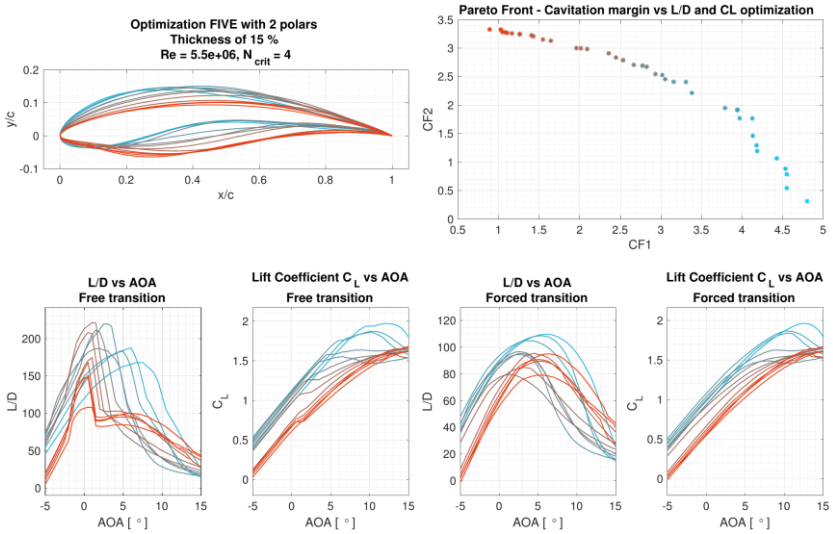

Fig. 4. Foils geometry, Pareto front, L/D and C_L obtained with optimization FIVE for t/c_{max} = 15%

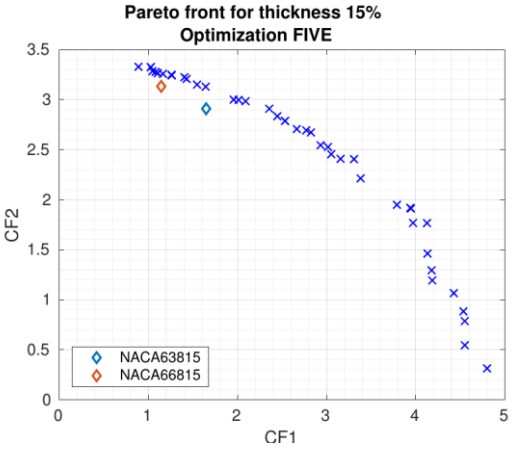

Fig. 5. Comparison with reference hydrofoils for t/c_{max} = 15%

L/D as well as optimum C_L, for both regimes, is higher. For example, hydrofoil 1 could have lower L/D in the clean regime than hydrofoil 2 but still have a higher value of CF1 value because it has higher L/D in the rough regime as well as optimum C_L for both regimes. Despite this fact, all foils on the Pareto front are optimal in a multi-objective sense: the red represent a design compromise with greater cavitation performance, whereas blue puts emphasis on hydrodynamic performance, as previously stated.

For all blade spanwise sections in Table II, results show similar trends, as illustrated in Fig. 4 to Fig. 11.

Regarding the geometry of the optimized hydrofoil

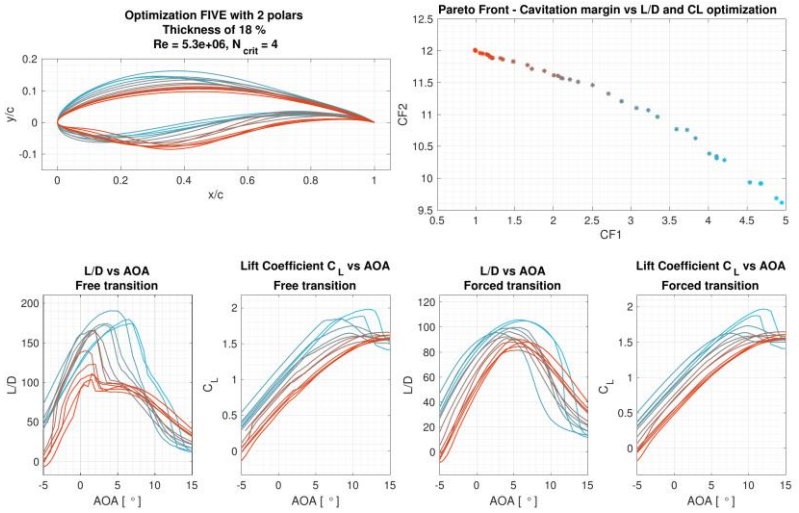

Fig. 6. Foils geometry, Pareto front, L/D and C_L obtained with optimization FIVE for t/c_{max} = 18%

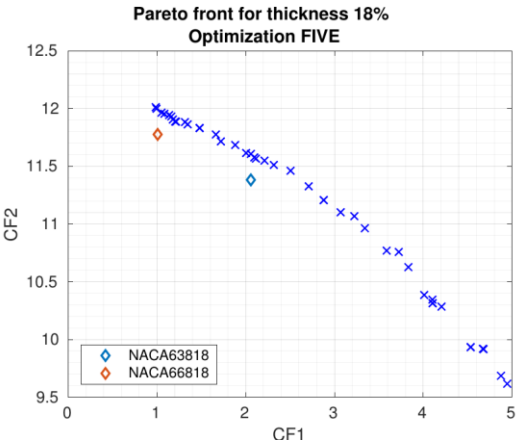

Fig. 7 - Comparison with reference hydrofoils for t/c_{max} = 18%

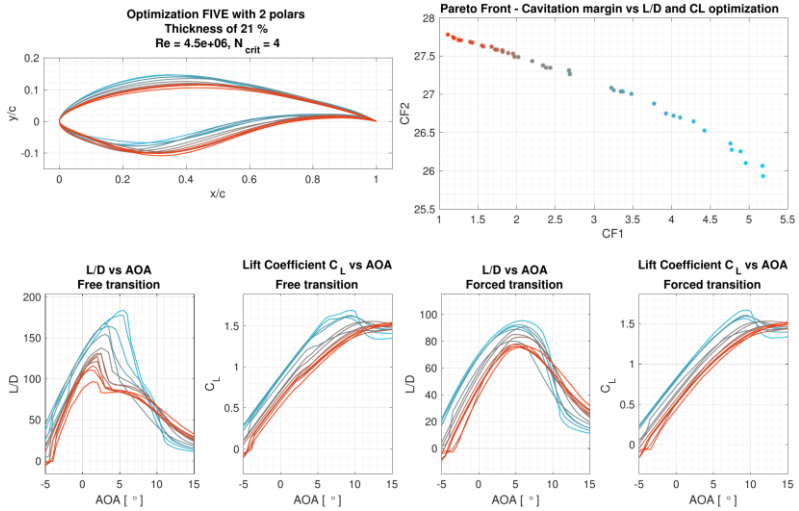

Fig. 8. Foils geometry, Pareto front, L/D and C_L obtained with optimization FIVE for t/c_{max} = 21%

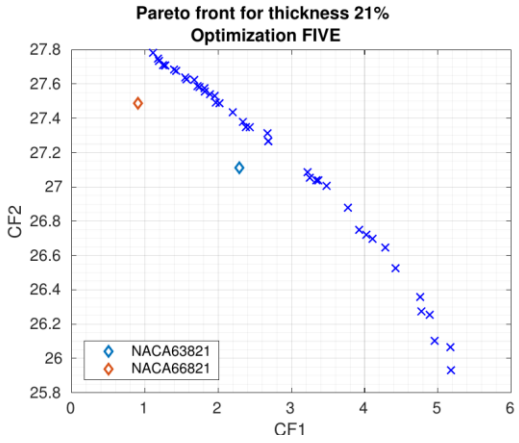

Fig. 9. Comparison with reference hydrofoils for t/c_{max} = 21%

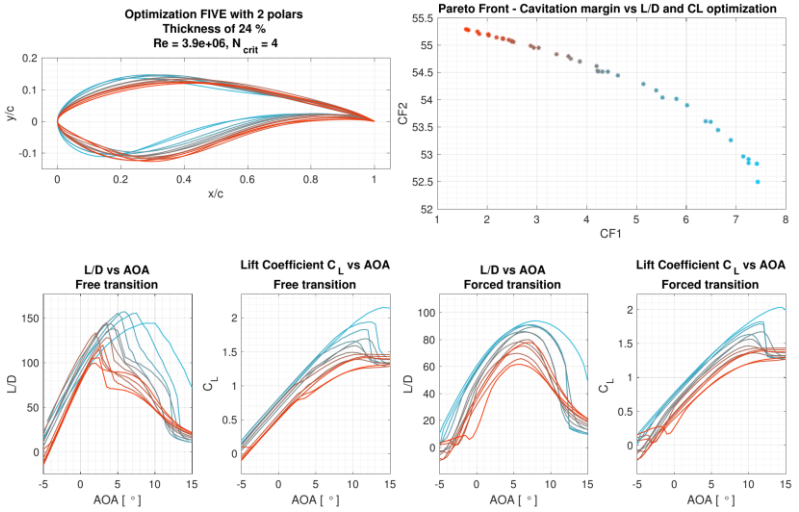

Fig. 10. Foils geometry, Pareto front, L/D and C_L obtained with optimization FIVE for t/c_{max} = 24%

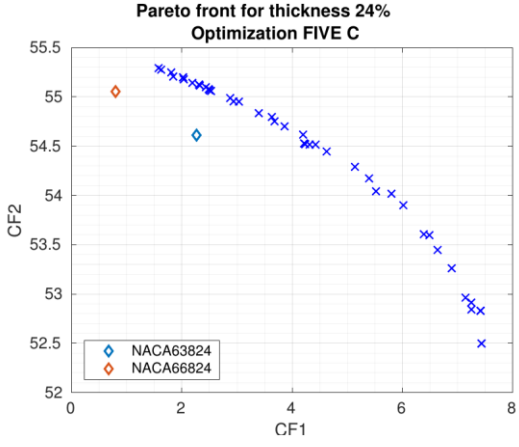

Fig. 11. Comparison with reference hydrofoils for t/c_{max} = 24%

sections, generally foils with higher CF1 (blue shapes) have a larger upper surface maximum thickness and are thus more cambered compared to the more cavitation-driven (red shapes) foils. One also notices the chordwise location of the maximum thickness t/c_{max} is generally located further aft (closer to the trailing edge) for the cavitation-driven foils. It is expected that both previously mentioned geometric features combined yield gradually weaker suction peaks, *i.e.* smaller magnitude $(-C_{p_{min}})$) as the cavitation margin increases, or in other words, as one goes from the blue towards the red foils. Still regarding the geometry, the lower surfaces of the foils show an S-shape towards the trailing edge, which is characteristic of energy harvesting foils [18]. This results in aft-loading and is consistent with a large $C_{L\,opt}$ value that is aimed for also in the current optimization effort.

The aforementioned geometric trends naturally correlate with the behaviour observed in the foils' polars. Specifically, more cambered foils have higher $C_L$values at a given AOA, at least up to stall ($\alpha_{Stall} \approx 10°$). The foils' polars also show that forced-transition does not significantly decrease the lift coefficient and lift-to-drag ratio, indicating the foils are relatively roughness-insensitive. Moreover one notices there is a moderate range of AOA, in the order of $\Delta\alpha = 3 - 5°$ over which the lift-to-drag ratio is plateauing, which meets the requirements imposed in the CF1 formulation.

As for the overall performance, we can observe from Fig. 7, Fig. 9 and Fig. 11 there are a number of optimized hydrofoils (represented with crosses) which outperform the reference hydrofoils obtained in each simulation. For example, for the same cavitation margin (same CF2 value *i.e.* along a horizontal line in the graph of figure Fig. 11) as the hydrofoil NACA 63-824, the corresponding optimized hydrofoil nearly doubles the value of the CF1, which may be interpreted as having a so-defined hydrodynamic performance nearly twice as good as the reference NACA foil. Specifically for this hydrofoil, an increase of 73% and 99% in maximum L/D and C_L, are obtained respectively, for the rough regime, whereas for the clean regime the maximum L/D increases by 5% and optimum C_L is 4% larger than for the reference NACA foil.

D. *Optimization of blade tip hydrofoils – improving t/c_{max} = 12%*

Since the section at r/R = 100% is the most prone to cavitation, additional optimizations are made in order to further improve the performance of the 12% thickness hydrofoil, while ensuring good cavitation performance. CF1 was adjusted for the blade-tip section optimization, according to:

$$C_{L_{new\,foil}}^{adim} = \left(\frac{C_{L_{new\,foil}}^{weighted} - C_L^{ref}}{C_L^{ref}} + 1\right)^3 \tag{17}$$

$$L/D_{new\,foil}^{adim} = \left(\frac{L/D_{new\,foil}^{weighted} - L/D^{ref}}{L/D^{ref}} + 1\right)^3 \tag{18}$$

Similarly to the previous CF1 version, the power 3 is used to "push" the optimization routine to further optimize the value of CF1, granting more sensitivity to the process. The other terms used to calculate CF1 remain as stated earlier.

CF2 for the blade-tip foil optimization is adjusted analogously:

$$CF2 = \left[\left(\left(\sigma_{r/R}\right)_{min} - \left(-C_{p_{min}}\right)_{max}\right) + 1\right]^3 \tag{19}$$

This alternative CF1 formulation (referred to as version 8 in the figures) successfully increases values of L/D for clean and rough regimes (see Fig. 12 and Fig. 13) compared to the CF1 formulation used (version 5) for the remaining blade sections

For the same cavitation margin as the reference hydrofoil NACA 63-812, the corresponding optimized hydrofoil (*i.e.* along a horizontal line on the graph of Fig. 13) displays improvements of 18% and 30% in maximum L/D and optimum C_L, respectively, for the clean regime; for the rough regime, there is an improvement of 11% in optimum C_L and a reduction of 8% in maximum L/D. For this optimization one of the reference hydrofoils is S1210 [19]. Optimization results show 6 novel foils that outperform S1210, all having greater cavitation margin

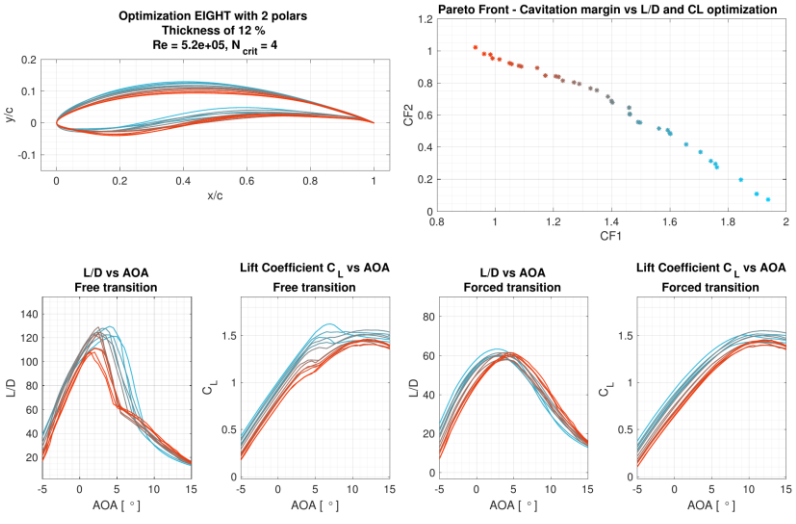

Fig. 12. Foils geometry, Pareto front, L/D and C_L obtained with optimization FIVE for t/c_{max} = 12%

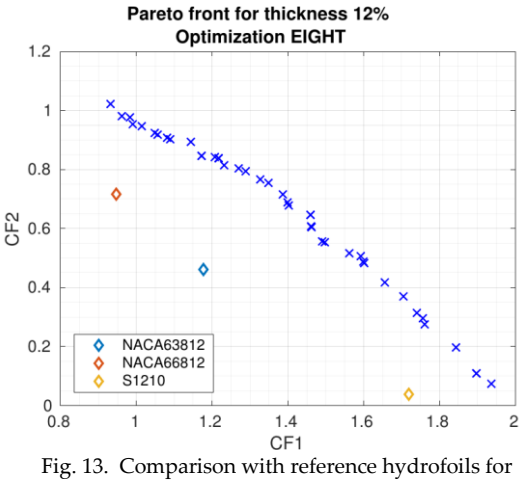

Fig. 13. Comparison with reference hydrofoils for t/c_{max} = 12%

(see Fig. 13). The first optimized hydrofoil (greater CF1 value in Fig. 13) improves the performance of S1210 by 13% and 12% in maximum L/D and optimum C_L, respectively, in clean regime. In rough regime there is a decrease of 2% in L/D and an increase of 3% in optimum C_L.

V. Selected Hydrofoils, IST-MT1-XX

The previous section presented 15 optimized foils per blade section, comprising the Pareto front. As such, all of the presented shapes are optimal in a multi-objective sense. The specific hydrofoil choice from the Pareto front for each relative thickness is made with the objective of employing these foil sections on a new HACT rotor (see [7],[15]). IST-MT1-XX is the name chosen for the hydrofoils, and stands for:

- *IST* - Instituto Superior Técnico, institution with which this article is produced;
- *MT1* - Marine Turbine, generation of hydrofoils 1;
- *XX* - Two digits denoting the maximum relative thickness of the hydrofoil in percentage. If t/c_{max} is 18%, the foil is named IST-MT1-18.

The criteria of selection for the hydrofoils is as follows:

- Similar optimum angle of attack between adjacent sections of the blade. The difference in optimum angle of attack should be small so the blade would be easier to manufacture; this also reduces spanwise flow components;
- High value of L/D, in order to obtain a greater energy conversion efficiency in turbine operation, translated in a higher value of power coefficient C_P. Hydrofoils were selected for their highest value of L/D in the clean regime (*i.e.* natural transition);
- Similarity of the hydrofoil geometry along the radius of the blade r, according to common practice [18]. This excludes geometries that deviate excessively from the remaining hydrofoils.

High cavitation margin is also required for each section, and thus this factor is also considered in the selection of each hydrofoil.

Fig. 14 displays the chosen hydrofoils according to the previously stated criteria along with: the pressure distribution C_p along chord x/c for the $\mathrm{AOA_{opt}}$ clean, *i.e.* the optimum angle of attack with natural transition; C_L vs AOA curves for both regimes, *i.e.* natural (free) and forced transition; L/D vs AOA curves for both regimes.

All data curves are calculated at the Reynolds number experienced by the foil at the section r/R as displayed in Table II. Table III displays relevant data regarding the selected hydrofoils. The Bernstein coefficients describing the geometry are given in appendix.

TABLE III
BLADE SECTION AND SELECTED HYDROFOILS DATA

Span r/R [%]	Foil at section	Maximum Thickness t/c_{max} [%]	Optimum **AOA** $\mathrm{AOA_{opt\ clean}}$ [°]	Optimum $\mathbf{C_L}$ $C_{L\ opt\ free}$	Maximum **L/D** $L/D_{max\ free}$
20	IST-MT1-24	24	5.5	1.45	164
30	IST-MT1-21	21	5.5	1.54	184
45	IST-MT1-18	18	4.0	1.61	191
75	IST-MT1-15	15	3.5	1.53	228
100	IST-MT1-12	12	2.5	1.16	131

From Table III we can observe that coherence between $\mathrm{AOA}_{opt\ clean}$ at each section was achieved, along with similar values of $C_{L\ opt\ free}$ along the blade span. From Fig. 14 we can also observe the gradual evolution of the various section contours along the span, with only IST-MT1-12 standing out. The lower surfaces are very similar for the different relative thicknesses. For the upper surface the foil contour is also similar, with a clear trend of maximum thickness moving aft as thinner sections are considered. These trends hold except for the tip-region foil, as already mentioned, which was obtained using a different optimization, owing to the larger risk of cavitation.

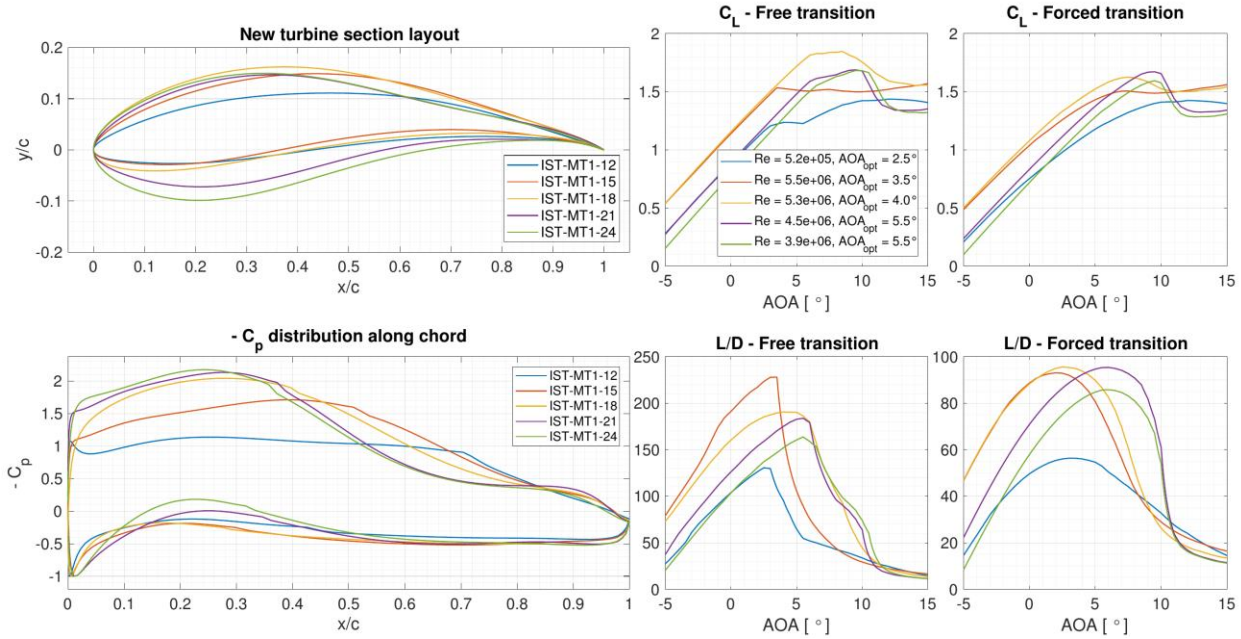

Fig. 14. Selected hydrofoils IST-MT1-XX

VI. CONCLUSIONS

The present study addressed the design and optimization of hydrofoils tailored for marine current turbines. An in-house optimization framework which uses CST for the foil geometry parametrization and a viscous-inviscid panel code to estimate foil hydrodynamic performance was employed. The optimization challenge was formulated as a multi-objective problem and solved with the NSGA-II genetic algorithm. Two specific hydrofoil performance cost functions were defined as design goals, contrasting hydrodynamic (CF1) with cavitation (CF2) performance.

The results of the hydrofoil optimization show similar trends for all the relative maximum thickness and correspondent HACT blade spanwise sections evaluated.

Regarding geometry, and as the Pareto front scores decrease in cavitation margin, *i.e.* CF2 value decreases and CF1 value increases, the maximum relative thickness chord-wise location moves towards the leading edge, along with an increase in camber. This is consistent with the current definition of hydrodynamic performance expressed by CF1, as greater camber induces stronger suction regions and thus renders larger C_L values. Conversely, as the cavitation margin increases, represented by CF2, the geometric trends produce a gradually weaker suction peak.

As for the foil lift and drag polars, the optimization ensures a good performance for a range of angles of attack around the optimum angle of attack, while being relatively insensitive to roughness.

In terms of overall performance and compared to reference hydrofoils, the optimized sections with equivalent cavitation margin display improvements in maximum L/D and optimum C_L of up to 66% and 23%, respectively, in the clean regime; in the rough regime, improvements in maximum L/D and optimum C_L reach values of 73% and 99%, respectively.

Considering both cost functions, the method employed yields a large number of hydrofoils per optimization, offering the possibility of choice between various levels of compromise between cavitation and hydrodynamic performance.

In general, the optimization results show that the optimized hydrofoils have better performance not only with natural (free) transition, clean regime, but also with forced transition, rough regime, demonstrating that the optimization setup, with the cost functions developed, is successfully implemented. This means that, if transition occurs, the optimized hydrofoils will still perform better than the reference sections for a range of angles of attack around the optimum.

Finally, one optimized foil section is chosen for each blade section. A total of five hydrofoils are selected with a blade design in mind, the IST-MT1-XX series. The selected foil distribution ensures a smooth geometry and comparable lift coefficient and optimum AOA throughout the blade.

As future work on the subject of design and optimization of hydrofoils tailored for marine current turbines, the authors would recommend:

- It is important to quantify the relevance of each transition regime: the amount of time that turbine blades operate with natural or forced transition is unknown. In the present study, equal importance, or weights, is considered for clean and rough regimes. Future studies could consider different weights for the free/forced transition regimes and investigate its impact on foil geometry and CF1, CF2 performance.

- A comprehensive analysis of roughness effects: studying the influence of roughness and optimizing hydrofoils and blades to counter its adverse effects may extend the range of operating conditions and prevent anomalous situations that could severely hinder the turbine operational performance; this study of roughness may prove important to adequately assess the effects of fouling.

ACKNOWLEDGEMENT

This work was supported by FCT/MCTES (PIDDAC) through project UID/EEA/50009/2019.

APPENDIX

TABLE IV
BERSTEIN COEFFICIENTS FOR HYDROFOIL IST-MT1-12

IST-MT1-12								
Upper	0.137	0.2645	0.2411	0.3546	0.1878	0.5669	0.2423	0.4151
Lower	0.1264	0.009127	0.2339	-0.222	0.1747	-0.3136	0.03398	-0.408
Trailing edge	0.0001							

TABLE V
BERSTEIN COEFFICIENTS FOR HYDROFOIL IST-MT1-15

IST-MT1-15								
Upper	0.2003	0.3581	0.2799	0.505	0.357	0.5721	0.2148	0.5782
Lower	0.1341	0.02235	0.2565	-0.3236	0.1911	-0.4328	-0.0297	-0.3938
Trailing edge	0.0003							

TABLE VI
BERSTEIN COEFFICIENTS FOR HYDROFOIL IST-MT1-18

IST-MT1-18								
Upper	0.2956	0.4033	0.3932	0.4846	0.4341	0.4126	0.2763	0.5803
Lower	0.1981	0.07704	0.1975	-0.241	0.201	-0.386	0.0298	-0.4849
Trailing edge	0.0003							

TABLE VII
BERSTEIN COEFFICIENTS FOR HYDROFOIL IST-MT1-21

IST-MT1-21								
Upper	0.2324	0.4115	0.2729	0.6241	0.186	0.349	0.2376	0.5819
Lower	0.211	0.1847	0.308	0.3406	0.07502	-0.3043	0.1288	-0.4376
Trailing edge	0.0002							

TABLE VIII
BERSTEIN COEFFICIENTS FOR HYDROFOIL IST-MT1-24

IST-MT1-24								
Upper	0.2925	0.3653	0.4172	0.4329	0.3683	0.2065	0.3682	0.4476
Lower	0.3005	0.2752	0.3639	0.0838	0.0829	-0.1379	0.04412	-0.4089
Trailing edge	0.0003							

REFERENCES

[1] U.S. Energy Information Administration, "Annual Energy Outlook 2011," 2011.

[2] The Executive Committee of Ocean Energy Systems, "An overview of Ocean Energy activities in 2017 - Annual Report," 2017.

[3] Z. Zhou, M. Benbouzid, J.-F. Charpentier, F. Scuiller, and T. Tang, "Developments in large marine current turbine technologies – A review," *Renew. Sustain. Energy Rev.*, vol. 71, pp. 852–858, May 2017.

[4] K. W. Ng, W. H. Lam, and K. C. Ng, "2002-2012: 10 Years of Research Progress in Horizontal-Axis Marine Current Turbines," *Energies*, vol. 6, no. 3, pp. 1497–1526, 2013.

[5] M. J. Khan, G. Bhuyan, M. T. Iqbal, and J. E. Quaicoe, "Hydrokinetic energy conversion systems and assessment of horizontal and vertical axis turbines for river and tidal applications: A technology status review," *Appl. Energy*, vol. 86, no. 10, pp. 1823–1835, 2009.

[6] G. de Oliveira, "Wind Turbine Airfoils with Boundary Layer Suction - A Novel Design Approach,", MSc thesis, Delft University of Technology, Delft, the Netherlands, 2011.

[7] F. Espenica, R. B. Santos Pereira, J. Baltazar, and J. A. C. Falcão de Campos, "Design of a reference horizontal axis marine current turbine with dedicated hydrofoil sections," Lisbon, submitted to *EWTEC 2019*, 2019.

[8] B. M. Kulfan, "A Universal Parametric Geometry Representation Method-"CST"," in *45th AIAA Aerospace Sciences Meeting and Exhibit*, 2007, pp. 1–36.

[9] G. de Oliveira, R. B. Santos Pereira, and U. Fechner, "Multi-objective airfoil design," *Airborne Wind Energy Conference*, 2017. [Online]. Available: http://awec2017.com/presentations/gael-de-oliveira. [Accessed: 26-Jan-2019].

[10] R. B. Santos Pereira, G. de Oliveira, W. A. Timmer, and G. J. W. van Bussel, "Design of HAWT airfoils tailored for active flow control," *Wind Energy*, 2017.

[11] R. B. Santos Pereira, "Active Stall Control of Horizontal Axis Wind Turbines - A dedicated study with emphasis on DBD plasma actuators,", PhD dissertation, Delft University of Technology, 2017.

[12] R. P. J. O. M. van Rooij, "Modification of the boundary layer calculation in RFOIL for improved airfoil stall prediction," Netherlands, 1996.

[13] R. B. Santos Pereira, G. De Oliveira, W. A. Timmer, and E. Quaeghebeur, "Probabilistic Design of Airfoils for Horizontal Axis Wind Turbines," p. 10, 2018.

[14] M. Drela and H. Youngren, "XFOIL - Subsonic airfoil development system," 2013. [Online]. Available: http://web.mit.edu/drela/Public/web/xfoil/. [Accessed: 04-Sep-2018].

[15] G. De Oliveira, R. Pereira, N. Timmer, and R. Van Rooij, "Improved airfoil polar predictions with data-driven boundary-layer closure relations," *J. Phys. Conf. Ser.*, vol. 1037, no. 2, 2018.

[16] F. Espenica, "Design and Optimization of Hydrofoils tailored for Marine Current Turbines,", MSc thesis, Instituto Superior Técnico, Lisbon, 2018.

[17] A. F. Molland, A. S. Bahaj, J. R. Chaplin, and W. M. J. Batten, "Measurements and predictions of forces, pressures and cavitation on 2-D sections suitable for marine current turbines," *Proc. Inst. Mech. Eng. Part M J. Eng. Marit. Environ.*, vol. 218, no. 2, pp. 127–138, 2004.

[18] W. A. Timmer and R. P. J. O. M. van Rooij, "Summary of the Delft University Wind Turbine Dedicated Airfoils," *J. Sol. Energy Eng.*, vol. 125, no. 4, p. 488, 2003.

[19] J. N. Goundar, M. R. Ahmed, and Y. H. Lee, "Numerical and experimental studies on hydrofoils for marine current turbines," *Renew. Energy*, vol. 42, pp. 173–179, 2011.

[20] R. Abadia, "Estudo de Perfis,", MSc thesis, Instituto Superior Técnico, Lisbon, 2007.

[21] R. P. J. O. M. van Rooij and W. A. Timmer, "Roughness Sensitivity Considerations for Thick Rotor Blade Airfoils," *ASME 2003 Wind Energy Symp.*, vol. 125, no. November, pp. 22–31, 2003.